Journal of
Engineering Sciences
Faculty of Engineering
Assiut University
JES
مجلة
العلوم الهندسية
كلية الهندسة
جامعة أسيوط
journal homepage: http://jesaun.journals.ekb.eg

Realistic Computational Modeling of Biothermal Effects Inside Human Head Exposed to Mobile Phone Radiation

Received 30 November 2022; Revised 10 January 2023; Accepted 10 January 2023

Ahmed S. Ramadan[1]
H. M. Shafey[2]
Nabil Y. Abdelshafe[3]
Ali K. Abdelrahman[4]

Keywords
Electromagnetic radiation, Heat transfer, Temperature distribution, Human head, Mobile phone

Abstract

The recent development of smartphones and the introduction of newer mobile phone networks led to increasing concerns over the prolonged exposure of delicate human organs to mobile phone radiation. This study investigates the Specific Absorption Rate (SAR) and temperature distributions inside anatomical head model exposed to mobile phone radiation. The effects of different microwave frequencies (0.9, 1.8, and 3 GHz) and different antenna positions (voice and video calling positions) were studied. The propagation, penetration, and absorption equations of the microwave radiation as well as the bioheat equation were numerically solved inside the computational domain. The numerical results of the present study were verified by comparison to other published numerical solutions. The Peak overall SAR and temperature rise were found in the voice calling position for the 3 GHz frequency as 14.9 W/kg and 1.6 °C, respectively. The model showed negligible peak SAR and temperature rise values for the video calling position. Moreover, the peak SAR and temperature rise locations are not correlated. Additionally, the temperature rise exceeded 63% of the final value at 6 minutes of exposure time for all the studied microwave frequencies.

Nomenclature

B	Magnetic induction vector, V.s/m^2	T	Temperature, °C
b	Magnetic induction through a cell facet, V.s	t	Time, s
c	Specific heat capacity, J/(kg.K)	W_c	Width of the computational domain, m

[1] ahmed.sameer.13@aun.edu.eg - Demonstrator, Dept. of Mechanical Power Eng., Assiut University, Assiut 71516, Egypt
[2] h_shafey@aun.edu.eg - Professor, Dept. of Mechanical Power Eng., Assiut University, Assiut 71516, Egypt
[3] nyassien@yahoo.com - Associate Professor, Dept. of Mechanical Power Eng., Assiut University, Assiut 71516, Egypt
[4] nada_ali54@yahoo.com - Professor, Dept. of Mechanical Power Eng., Assiut University, Assiut 71516, Egypt

https://doi.org/10.21608/JESAUN.2023.177825.1186

D	Electric displacement vector, C/m^2	*Greek letters*	
d	Electric displacement through a cell facet, C	α	Blood perfusion coefficient, $W/m^3.K$
E	Electric field intensity vector, V/m	α_a	Natural convection coefficient, $W/m^2.K$
e	Electric voltage along cell edge, V	ε	Material Permittivity, F/m
f	Electromagnetic wave frequency, Hz	θ	Orientation of the antenna
H	Magnetic field intensity vector, A/m	μ	Material Permeability, H/m
h	Magnetic voltage along the edge, A	ρ	Density, kg/m^3
J	Current density vector, A/m^2	σ	Electric conductivity, S/m
j	Current density through a cell facet, A	*Subscripts*	
k	Thermal conductivity, W/(m.K)	a	Antenna
L_c	Length of the computational domain, m	b	Blood
m	Magnetization of a cell material, A	c	Computational domain
N_p	Number of computational nodes	h	Head
p	Electric polarization through a cell facet, C	i	Incident
q	Free charge density, C/m^3	m	Metabolic
q_m	Metabolic heat generation, W/m^3	r	Relative
S_c	Height of the computational domain, m	x, y, z	Cartesian Coordinate Axes

1. Introduction

The widespread usage of mobile phones raises concerns over the influence of mobile phone microwave radiation on exposed human body especially sensitive organs such as the brain. To control the allowable amount of absorbed energy inside human tissues, Electromagnetic (EM) radiation is regulated by the peak Specific Absorption Rate (SAR) and peak temperature rise which are determined by reputable organizations such as the International Commission of Non-Ionizing Radiation Protection (ICNIRP) [1] and the Institute of Electrical and Electronics Engineers (IEEE) [2]. The main effect of mobile phone radiation absorption is temperature rise inside the tissue. This temperature rise can result in serious physiological issues for the internal sensitive organs [3]. For example, a temperature rise inside the brain can lead to brain lesions, and a small rise of about 1 °C can alter the production of hormones, suppress the immune response, and lead to changes in behavior [4].

Although SAR is a parameter used to quantify the allowable amount of absorbed radiation energy, it is not sufficient to fully understand the effects of EM radiation interaction with the human body. Therefore, a coupled electromagnetic-thermal analysis gives a more comprehensive understanding of this physical phenomenon. There are many factors that affect the distribution and amount of absorbed radiation energy resulting from exposure to mobile phone radiation. The frequency of the microwave radiation, the position of the mobile phone antenna relative to the human head, exposure time, the

human head geometry and dimensions, the dielectric and thermophysical properties of the head tissue materials, the biological processes such as blood circulation, and the anatomical structure of the human head are among the factors affecting the absorbed radiation energy [5].

For the last few decades, many studies [6 – 14] explored the interaction of mobile phone radiation with human tissues focusing on the electromagnetic perspective. Other studies [15 - 24] constructed coupled electromagnetic-thermal mathematical models. Bhargava et al. [25] performed a computational analysis on the characteristics of high-power microwave radiation absorption inside a simplified three-dimensional heterogeneous physical model of the human head. They studied the influences of head-mobile phone gap distance, human age, and microwave radiation energy on the SAR and temperature distributions at 900 MHz frequency. Stanković et al. [26] determined the distributions of absorbed energy and temperature inside a human child's head illuminated by a 900 MHz mobile phone radiation. Wessapan et al. [27] investigated the SAR and heat transfer inside a 2D physical model of the human body with internal organs exposed to near-field and far-field radiation. Seetharaman et al. [28] analyzed the effects of mobile phone radiation on SAR and heat transfer inside the human head. Their study is based on three-layer human head model that is exposed to different frequencies of different mobile phone technologies such as Wi-Fi and Bluetooth. Lwin et al. [29] performed a numerical analysis of a 2D simplified human head model exposed to mobile phone radiation. They investigated SAR and temperature distributions at frequencies ranging from 300 to 1800 MHz.

Table 1 Comparison between the present study and selected published research works.

Research work	Head model	Multiple frequencies	Different antenna positions	Frequency-dependent dielectric properties
Bhargava et al [25], 2019	Non-anatomically accurate multilayer (constant thickness) head		**X**	
Stanković et al [26], 2017	Anatomically accurate head			
Wessapan et al [27], 2018	2D human body	**X**		
Seetharaman et al [28], 2022	Three-layers head	**X**		**X**
Lwin et al [29], 2019	2D simplified head	**X**		**X**
Present study	Anatomically accurate head	**X**	**X**	**X**

The previous research works mostly used a simple multilayer human head model and sometimes a simpler 2D human head model. Moreover, there are significant variations in the computed results (SAR and temperature) of these research works which could be attributed to many factors including the used physical model, antenna radiated power, antenna-to-head distance, etc. These significant variations of the computed results are also confirmed by the latest published ICNIRP guidelines [1]. Based on the above discussion, there is a need to perform more realistic and accurate computational analysis of the mobile phone radiation interaction with the human head. This needed analysis should cover a wide range of conditions such as different operating frequencies and different usage patterns of the mobile phone.

The purpose of this paper is to study the effects of mobile phone radiation on an anatomically realistic human head model. Different microwave frequencies (0.9, 1.8, and 3 GHz) and different antenna-to-head positions (8 mm voice calling position and 150 mm video calling position) were investigated. The dielectric properties of the human head tissues are varied with the operating frequency to further improve the results' accuracy. The interaction of the mobile phone radiation with the human head is present as SAR and temperature distributions. Finally, this numerical model is verified by comparison with other well-established numerical solutions, using simplified physical model, to ensure confidence in its computational results. Table 1 shows a comparison of the present study with some selected published research works.

2. Formulation and Solution of The Computational Model

The present mathematical model is characterized by two sets of governing equations. The first set governs the steady propagation, penetration, and absorption of mobile phone radiation. The second set of equations governs the unsteady thermal energy balance inside the various tissues of the human head, including the absorbed mobile phone radiation. The term unsteady means that there are significant time variations of the dependent function on the macroscopic level. On the other hand, the term steady means no macroscopic time variations. This may be considered with two distinct cases: a fixed function with time and a periodic wave function that varies with time only on the microscopic level.

2.1 Conceptual Model

The conceptual model describes the real situation necessary for accurate formulation of the governing equations of the mathematical model. Figure 1 shows the main features of the conceptual model. Figure 1(a) illustrates the origin of the cartesian coordinates and the main dimensions of the whole computational domain in which the mobile phone radiation propagates. The outer imaginary boundaries of the whole computational domain enclose the human head and the antenna which represents the emitting part of the mobile phone. The patch antenna, which generates randomly polarized microwave radiation from its whole surface, has a general location (x_a, y_a, z_a) and a general orientation (θ). Figure 1(b) shows the trace of the generated microwave as it propagates out of the antenna and penetrates the different tissues of the human head where its energy may be absorbed. Figure 2 shows the important head important tissues constituting the main anatomical structure of the real human head. The tissues of human head generally, have different dielectric and thermophysical properties.

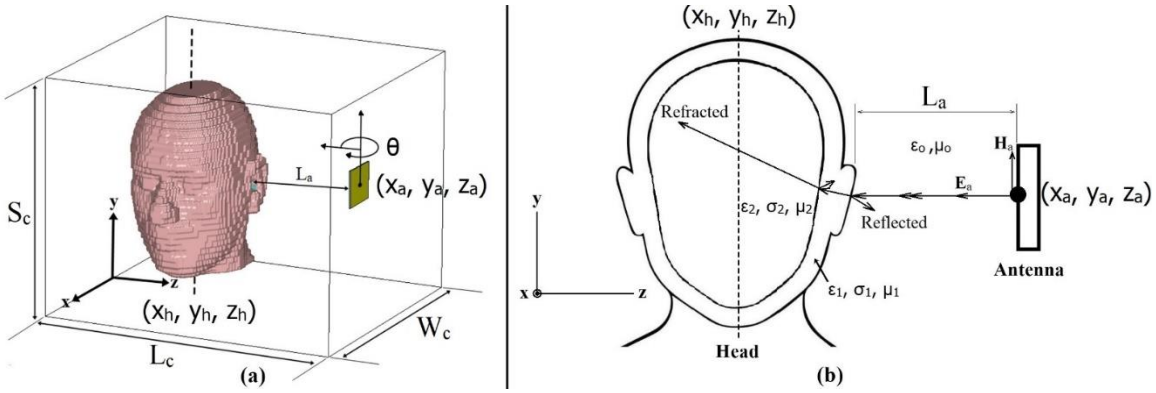

Fig. 1. Main features of the conceptual model: (a) The computational domain and the coordinate system, and (b) EM wave propagation and refraction.

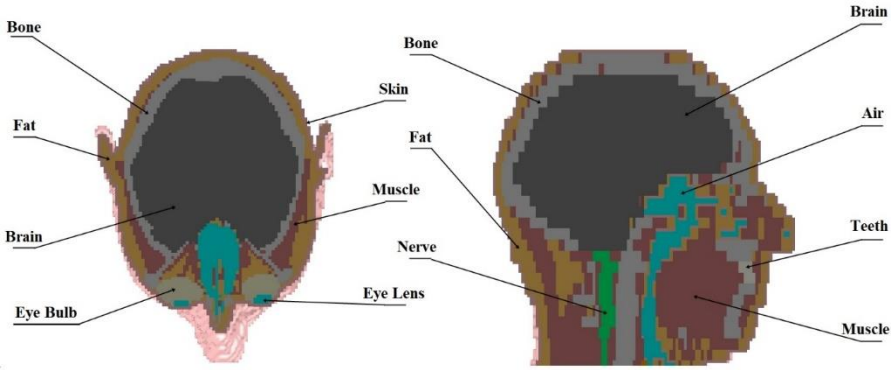

Fig. 2. Main structural tissues of the proposed human head related to the conceptual model.

2.2 Main Assumptions

- The electromagnetic field propagates in the three-dimensional space of the computational domain.
- The thermal energy balance is three-dimensional and is based on unsteady conditions during the exposure period.
- The free space is truncated by an absorbing boundary condition implementing the perfectly matched layer.
- The dielectric properties of the different tissues of the head are functions only of the microwave frequency.
- The thermophysical properties of the head tissues are considered constant because of the small temperature variations since the amount of heat generated is not enough to alter these properties.
- The thermal energy term due to physical phase change of the material state is neglected.

2.3 Electromagnetic Propagation Equations

The generated microwaves in a medium are mathematically described by Maxwell's equations [30]. These Maxwell equations are based on two groups of vectors [31]. The first group constitutes the two basic vectors representing the electric field intensity vector **E** and the magnetic induction density vector **B**. The second group constitutes the three additional vectors represents the magnetic field intensity vector **H**, the electric displacement vector **D**, and the electric current density vector **J**. The last three vectors, which are related to the first group of vectors, describe the influence of the head tissues through which the Electromagnetic wave propagates and penetrates.

Applying the Finite Integration Technique (FIT) [32] on the integral form of Maxwell equations produces a group of matrices of scalar variables. These scalar variables, denoted by e, h, b, d, and j, represent the integration of the three components of the corresponding five wave vectors (**E**, **B**, **H**, **D**, and **J**, respectively) along the edges or over the areas of the discretized cells. The resulting equations are the four Maxwell Grid Equations (MGE) and the three material equations. The Maxwell grid equations [32] are given by

$$\left[\dot{C}\right]_{N_p\times 3N_p}[\hat{e}]_{3N_p\times 1} = -\frac{\partial}{\partial t}\left[\hat{\hat{b}}\right]_{N_p\times 1} \tag{1}$$

$$\left[\tilde{C}\right]_{N_p\times 3N_p}[\hat{h}]_{3N_p\times 1} = \frac{\partial}{\partial t}\left[\hat{\hat{d}}\right]_{N_p\times 1} + [\hat{j}]_{N_p\times 1} \tag{2}$$

$$\left[\tilde{S}\right]_{N_p\times 3N_p}\left[\hat{\hat{d}}\right]_{3N_p\times 1} = [\mathrm{q}]_{N_p\times 1} \tag{3}$$

$$\left[\acute{S}\right]_{N_p\times 3N_p}\left[\hat{\hat{b}}\right]_{3N_p\times 1} = 0, \tag{4}$$

where $\dot{C}$ and $\tilde{C}$ represent the discrete curl matrix on the grid and the dual grid, respectively [32]. The symbols $\acute{S}$ and $\tilde{S}$ represent the discrete divergence matrix on the grid and the dual grid, respectively [32]. N_p is the number of nodes inside the computational domain. The term q represents the Free charge density (C/m^3). The three associated material equations [32] are given by:

$$\left[\hat{\hat{d}}\right]_{N_p\times 1} = [\varepsilon]_{N_p\times N_p}[\hat{e}]_{N_p\times 1} + \left[\hat{\hat{p}}\right]_{N_p\times 1} \tag{5}$$

$$[\hat{j}]_{N_p\times 1} = [\sigma]_{N_p\times N_p}[\hat{e}]_{N_p\times 1} \tag{6}$$

$$\left[\hat{\hat{b}}\right]_{N_p\times 1} = [\mu]^{-1}_{N_p\times N_p}\left[\hat{h}\right]_{N_p\times 1} + [\hat{m}]_{N_p\times 1}, \tag{7}$$

where the quantities $\varepsilon, p, \sigma, \mu, and$ m are the matrices of permittivity, Polarization, electric conductivity, magnetic permeability, and magnetization, respectively. These quantities are measured by F, C, S, H, and A, respectively.

The time derivatives ($\frac{\partial}{\partial t}\hat{\hat{b}}\ and\ \frac{\partial}{\partial t}\hat{\hat{d}}$) in eq. (1, 2) represent microscopic time changes in the order of the reciprocal of the microwave frequency 1/f (f = 0.9: 3 GHz). Accordingly, these time derivatives are treated numerically considering finite time differences in the order of picoseconds. The discretized form of the time derivatives can be obtained using the central finite-difference approximation. The associated initial conditions of the scalar variables e, h, b, d, and j are zero for all nodes of the computational domain.

The boundary conditions associated with the above Maxwell and material equations can be classified as outer boundary conditions and inner boundary conditions. The outer boundary conditions, corresponding to the cells at the boundaries of the computational domain, are specified as open boundaries which implements the Perfectly Matched Layers (PML) scheme. PML absorbs the propagating electromagnetic waves by acting as an imaginary anisotropic material. The inner boundary conditions, corresponding to the cells at the antenna surface, are characterized by Perfect Electric Conductor (PEC) boundary condition:

$$\boldsymbol{E_t} = 0 \tag{8}$$

Additionally, the head model boundary and the inter-tissue boundaries are described as continuous boundaries (energy conservation is applied at the boundary) and are mathematically expressed as follows:

$$\boldsymbol{E}_{t1} = \boldsymbol{E}_{t2} \tag{9}$$

The Specific Absorption Rate (SAR) represents the main output of the solution for Maxwell equations. The point SAR, at each cell of computational domain, is defined as the rate at which radiation energy per kilogram of the penetrating microwave is absorbed by a tissue. The expression of SAR may be obtained by normalizing the corresponding rate of the absorbed radiation energy per unit volume by the material density. This expression can be written in terms of the magnitude of the local electric field intensity vector |E| as:

$$SAR = \frac{\sigma\ |E|^2}{\rho}, \tag{10}$$

where σ is the dielectric conductivity, ρ is the tissue density.

Even that point specific absorption rate is used in many studies, most of the organizations' standards use a more practical averaged value of the specific absorption rate, SAR_{mg}. This value is the average of the point SAR for all cells included in the mass sample centered around the specified location. This mass sample could be 1 gram or 10 grams. In this study the mass sample is 10 g, hence SAR_{10g}.

2.4 Bioheat Equation

To get a complete understanding of the effects of microwave radiation on human head, heat transfer inside the biological tissues should be coupled with the electromagnetic analysis since the absorbed microwave radiation energy is converted to thermal energy inside the tissues. Penne's bioheat equation [33] is used to describe the unsteady three-dimensional thermal energy balance inside the head model. This equation is numerically solved using FIT space discretization technique similar to the discretization of Maxwell's equations [32],[33] as follows

$$\begin{aligned}[\rho c]_{N_p\times N_p}\frac{d}{dt}[T]_{N_p\times 1} &= -\left[\tilde{S}\right]_{N_p\times N_p}[k]_{N_p\times N_p}\left[\tilde{S}^T\right]_{N_p\times N_p}[T]_{N_p\times 1}\\ &+ [\alpha]_{N_p\times N_p}\left([T_b]_{N_p\times 1}-[T]_{N_p\times 1}\right)+[q_m]_{N_p\times 1}\\ &+ [\rho]_{N_p\times N_p}[SAR]_{N_p\times 1},\end{aligned} \tag{11}$$

The term on the left-hand side of eq. (11) expresses the transient thermal energy storage. The first term in the right-hand side expresses heat transfer by conduction, the second term expresses the heat transfer between the blood and the tissue (blood perfusion) with the blood temperature T_b is set to equal to the normal value of 37°C, the third term q_m expresses the metabolic thermal energy generation, while the fourth term expresses the thermal generation due to the mobile phone radiation. The symbols ρc, k, α, and ρ are the specific heat-density matrix (J/(m^3.K)), thermal conductivity matrix (W/(m.k)), volumetric convective heat transfer coefficient matrix (blood perfusion coefficient matric) (W/(m^3.K)), tissue density matrix (kg/m^3), respectively. While $\tilde{S}^T$ is the discrete gradient matrix [32]. keeping in mind, the macroscopic scale of unsteady temperature time variation, the temperature time derivative ($\frac{\partial T}{\partial t}$) is treated numerically considering finite time differences in the order of seconds. The boundary conditions associated with the bioheat equation are obtained by considering that each boundary cell, on the surface of the human model, is exposed to convective heat transfer to the surrounding ambient air in the computational domain according to the following equation:

$$-\mathrm{n}.(k\nabla T) = \alpha_a(T - T_a) \tag{12}$$

The heat transfer coefficient corresponding to free convection α_a has a constant value of 5 W/(m^2.K) [34]. The surrounding ambient air is assumed to have a constant temperature T_a= 25°C. The initial temperature distribution associated with eq. 11 is determined by performing the numerical solution of the special case of the bioheat equation obtained by omitting the left-hand side time dependent term and the thermal energy generation term ($[\rho][SAR]$), and with the same mentioned ambient and boundary conditions.

2.5 The Numerical Solution Procedure

All of the above matric equations can be numerically solved simultaneously in conjunction with the mentioned initial and boundary conditions using direct or iterative methods depending on the microwave frequency. The present solution procedure utilizes CST Microwave Studio software package [35] to perform the computations of the model. The solvers accuracy (allowable error) is 10^{-4} % of steady state electromagnetic wave energy. The computational domain is discretized using hexagonal mech cells whose size and number depend on the operating frequency and the geometry of the objects (head and antenna) inside the computational domain. A mesh study is performed to identify the appropriate number of cells that is required to achieve results accuracy independent of the grid discretization. The appropriate number of cells is the minimum number of cells which will not result in any tangible numerical errors due to the spatial discretization of the computational domain. Figure ٣ shows the results of such study applied to the case of the head exposed to microwave radiation at 0.9 GHz frequency from an antenna at 8 mm gap distance (voice calling position). The figure shows the change in peak temperature rise as the number of cells is changed for five locations. Each location is the peak temperature rise at a different tissue. We selected five different points for the mesh study to make sure that the results' accuracy is independent of the cell number at all regions of the head and for all the tissues. It is notable that at 2,000,000 cells the results are independent from the number of cells for all the tissues.

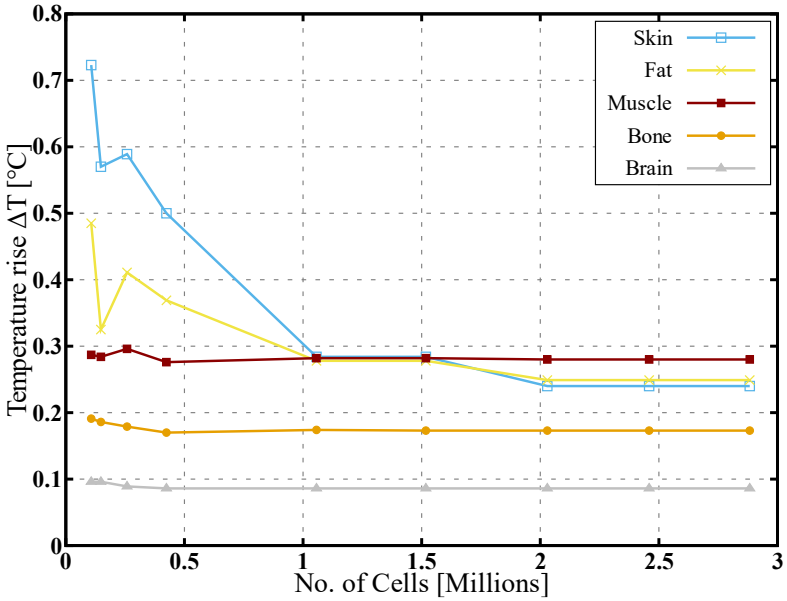

Fig. 3. Convergence curve of the computational grid.

3. Results and Discussion

In the present analysis, the governing equations of the proposed electromagnetic-thermal computational model were solved using FIT. The antenna radiated power is fixed at the average value of 1W as a worst-case scenario. A 1W antenna radiated power also have the added benefit

of easy prediction of the results at other radiated antenna power values, since the results are linearly related to the antenna radiated power value [25]. The linear relationship between the antenna and the computational results is due to the constant values of the dielectric and thermophysical properties at the considered frequencies normally used in the mobile phone communication systems. The effects of the mobile phone radiation are presented by the computed results of SAR_{10g} distributions as well as temperature history (variation with time) and distributions (variation with space at the end of exposure time) inside the human head model.
The numerical results are obtained for selected real exposure conditions covering the possible ranges of important parameters. Among these parameters are the antenna-to-head position (orientation and distance), and microwave frequency range. A 3D realistic human head model, obtained from medical studies [35] that used Magnetic Resonance Imaging (MRI) to determine the anatomical structure of the head, was selected for this study with dimensions shown in fig. 4. Table (2) presents the dielectric and thermophysical properties of the adult head model used in this analysis [36]. Three different frequencies are selected to be studied as they suit the aim of the study. Two different antenna positions were selected to simulate the common usage patterns of the mobile phone. In the first position (voice calling position), the antenna is located vertically at a horizontal distance of 8 mm from the ear of the human head model. In the second position (video calling position), the antenna is located vertically at a horizontal distance of 150 mm from the tip of the nose of the human head model. For convenience, the following discussion is classified into four distinct groups. The purpose of the first group is to verify the proposed numerical model through the comparison with other well-establish solutions. The second group is concerned with two-dimensional contour plots for the results of SAR_{10g} and temperature distributions. The third group focuses on the line plots of these results including the temperature history. The fourth group presents the bar charts describing the status of some important results for all microwave frequencies. These results are the peak values for SAR_{10g} and the peak temperature rise values.

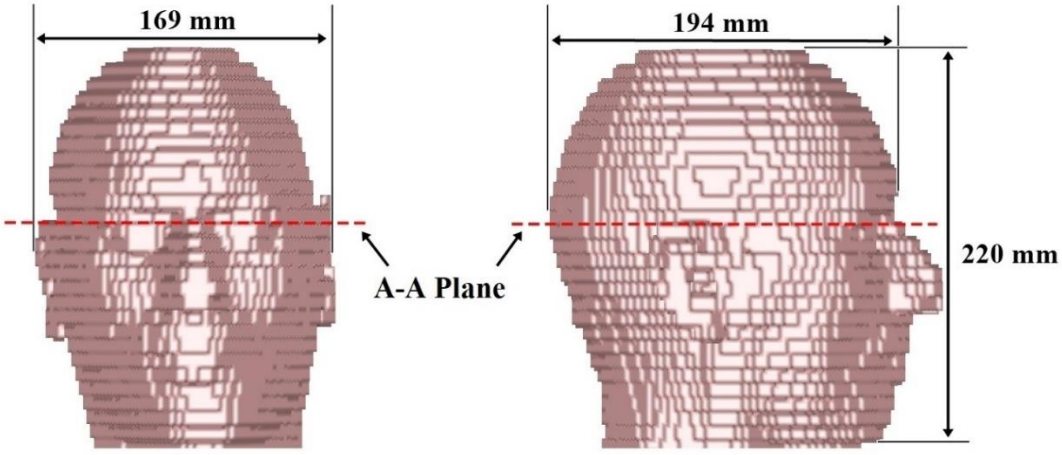

Fig. 4. Main dimensions of the adult human head model used in the present study.

Table 2: The dielectric and thermophysical properties of the adult's head tissues [36].

No.	Tissue	Dielectric properties						Thermophysical properties		
		0.9 GHz		1.8 GHz		3 GHz				
		ε_r	σ (S/m)	ε_r	σ (S/m)	ε_r	σ (S/m)	c (J/(kg.K))	k (W/(m.K))	ρ (kg/m^3)
1	Air	1	0	1	0	1	0	1000	0.02	1
2	Bone	20.8	0.34	19.3	0.588	17.9	1.01	1300	0.4	1850
3	Brain	45.8	0.816	43.55	1.152	41.75	1.865	3700	0.5	1045
4	Eye bulb	68.9	1.636	68.6	2.03	67.8	2.96	3900	0.6	1010
5	Eye lens	35.7	0.485	34.6	0.787	33.4	1.39	3700	0.4	1090
6	Fat	11.33	0.109	11	0.19	10.7	0.344	2500	0.2	900
7	Muscle	55	0.943	53.5	1.34	52.1	2.14	3500	0.5	1080
8	Nerve	32.5	0.574	30.9	0.843	29.6	1.33	3700	0.5	1080
9	Skin	41.41	0.867	38.9	1.18	37.5	1.74	3500	0.3	1100
10	Teeth	12.5	0.143	11.8	0.275	11.1	0.506	1300	0.4	2200

3.1 Verification of The Present Solution Procedure

Due to the illegal and unethical issues of exposing human bodies to electromagnetic radiation for experimental purposes, it is not possible to experimentally validate the computed results of the present model. However, the present numerical solution is verified by comparing its numerical computations with those of the well-establish numerical solution of Nishizawa and Hashimoto [37]. Their numerical solution is based on the method of moments (MOM) for the calculation of the electric field inside the human body. The physical model of the human body used by Nishizawa and Hashimoto's solution is replicated in the present solution for verification purposes and is shown in fig. 5. This model is a 2D body with elliptical horizontal cross-section, resembling the human body, consisting of 3 layers (skin, fat, and muscle) illuminated by a 1.3 GHz plane wave with a power density of 10 W/m^2 and propagating in the x direction. Figure 5 also shows the plots of the numerical computations used for the comparison between the present solution and the Nishizawa and Hashimoto's solution. These plots consider the point SAR distributions in the horizontal plane of the body model. The plots show good quantitative and qualitative agreement between the published solution and the present solution, except small-averaged errors. These agreements support both correctness and accuracy characteristic of the present solution procedure verification. Despite the verification model being simple, the utilization of the well-known CST modeling platform leads to confidence in the computational results of the more complex anatomical head model.

3.2 Contour Plots of SAR_{10g} and Temperature Distributions

Figure 6 shows the results for the effect of antenna microwave frequency on the contour distributions of SAR_{10g} in a horizontal plane passing through the center of the vertical antenna located at the voice calling position. It is evident that SAR_{10g} begins with its peak value located on the portion of head boundary closest to the antenna position and then decreases rapidly as the microwave radiation penetrates the head. This is true for all microwave frequencies. It is also

clear that the peak value of SAR_{10g} increases with the increase of the microwave frequency. One can define the penetration depth as the longest distance traveled by the microwave radiation through the human head after which the values of SAR are negligible (until it reachs 13.5% of the peak value). Accordingly, SAR_{10g} contours illustrate that the penetration depth decreases as the microwave frequency is increased. This behavior is expected since the penetration depth for each tissue medium mainly increases as the wavelength of the microwave increases, and by turn decreases with its frequency [38]. It is worth noting that the variation of SAR_{10g} contour distribution is due to the significant combined effects of the value of microwave frequency, and the dependence of the dielectric properties of each tissue on the frequency. The peak value of SAR_{10g} for the head model ranges from 2.58 to 14.9 W/kg with changing the frequency from 0.9 to 3 GHz.

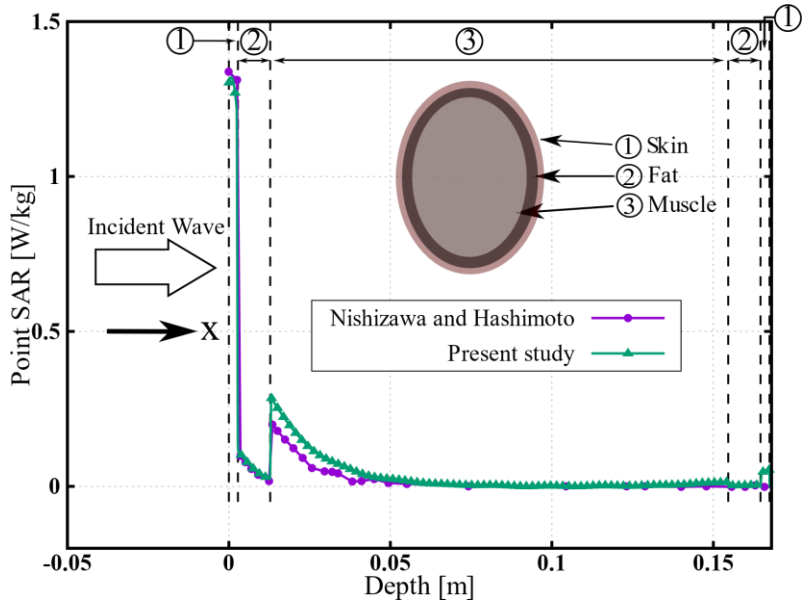

Fig. 5. Comparison of the numerical computations of the proposed method and those obtained by Nishizawa and Hashimoto's well-established model as well as the used physical model.

The numerical values of the SAR_{10g} with the antenna at the video calling position were obtained and found to be small compared to the values at the voice calling position. Therefore, these small values of SAR_{10g} at the video calling position cannot be clearly presented as contour distributions with the same scale of the results shown in fig. 6. Table (3) shows a comparison of the peak SAR_{10g} values for the head model at the voice and video calling positions. The indicated SAR_{10g} values clearly illustrate the significant reduction in SAR_{10g} values for the video calling position by two orders of magnitude compared to voice calling position. Also, there is a considerable reduction in the solid angle subtended by the head boundary surface when changing from the voice calling position at 8 mm to the video calling position at 150 mm. This reduction in the solid angle is associated with small electric field values due to the transition from the near field region in the case of voice calling position to the far field region in the case of video calling position. The small electric field values of the video calling position results in small SAR_{10g} values, compared with those of the voice calling position.

Figure 7(a) shows the results for the effect of antenna microwave frequency on the temperature contour distributions associated with the SAR_{10g} contour distributions shown in fig. 6 for the antenna in the voice calling position. Figure 7(b) shows the initial temperature distribution inside the human head model. According to the discussion on the results in table (3), one can expect the corresponding temperature distributions for the video calling position to be almost coincident with the initial temperature distributions shown in fig. 7(b). The peak temperature is a result of the combined effects of heating and cooling due to microwave radiation absorption, metabolic heat generation rate, blood perfusion rate, and convective heat transfer at the boundary of the head model. It is shown that as the microwave frequency increases the peak temperature increases, but at the same time the temperature of the inner organs, mainly the brain, decreases due to the reduction of the penetration depth as the microwave frequency increases. The peak temperature is 38.15 ℃ for the 3 GHz frequency and located on the ear as shown in fig. 7(b).

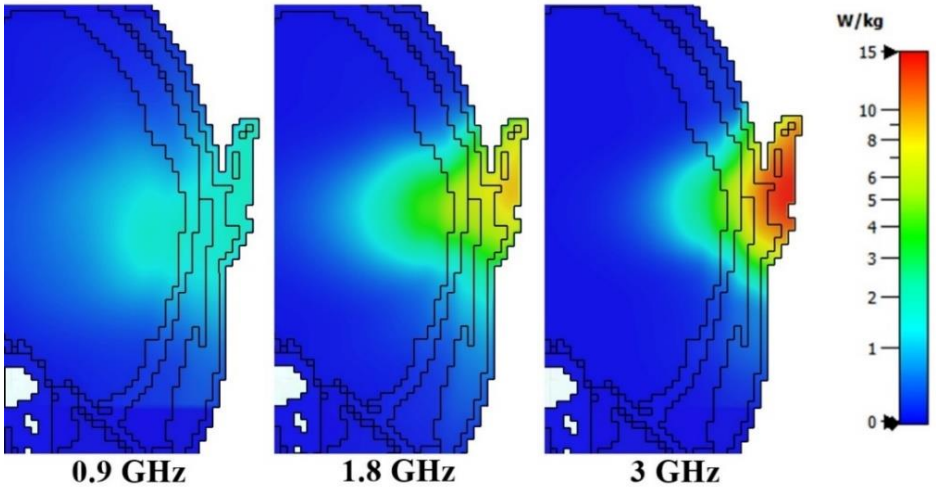

Fig. 6. Effect of microwave frequency on SAR_{10g} contour distributions in the horizontal plane A-A (shown in fig. 4) for the voice calling position.

Table 3: Comparison of peak SAR_{10g} numerical computations for the two antenna positions as well as the tissue in which the peak value is located.

Position	SAR_{10g} (W/kg)		
	0.9 GHz	1.8 GHz	3 GHz
Voice calling position	2.58 (skin)	9.25 (skin)	14.9 (skin)
Video calling position	0.4226 (skin)	`0.662 (skin)	0.721 (skin)

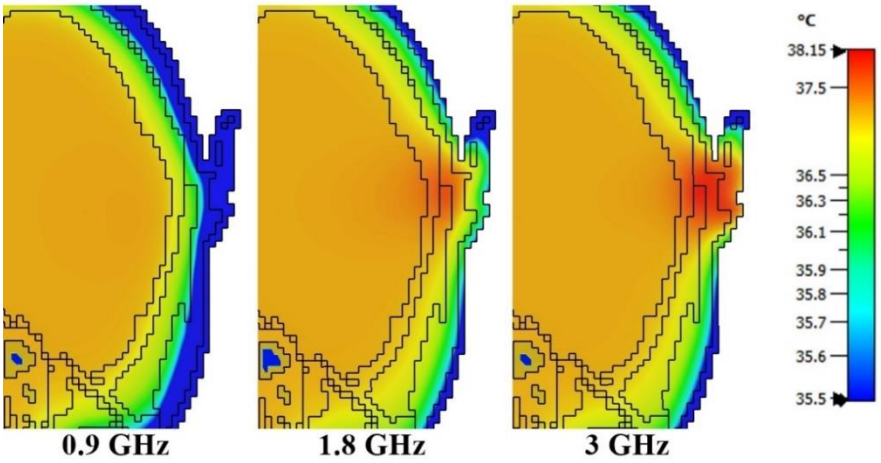

Fig. 7(a). Effect of microwave frequency on temperature contour distributions in the horizontal plane A-A (shown in fig. 4) in the voice calling position for 30-minute exposure period.

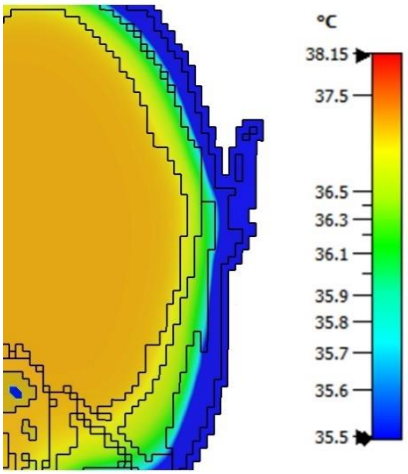

Fig. 7(b). Initial temperature distributions inside the head model at A-A (shown in fig. 4) plane.

Figure 7(a) also indicate that the locations of the peak SAR_{10g} and the peak temperature points are not correlated for the lower frequencies. This is due to the relatively low contribution of the small quantity of the absorbed radiation energy of the lower frequencies compared to the other factors in the thermal energy balance, as well as the effect of the thermophysical properties of each tissue. However, for the higher frequencies the two points are correlated since the large quantity of the absorbed radiation energy dominate the thermal energy balance and overcome the influences of the other factors.

3.3 Line Plots of SAR_{10g} and Temperature Computational Results

Figures 8 and 9 show the plots of the line distributions (1D) for both SAR_{10g} and the temperature. These plots support the above discussed contour distributions and clarify the quantitative description of these physical quantities. Figure 8 clearly indicates different peak values of SAR_{10g} for the different frequencies at the same location inside the fat tissue about 3 mm apart from the

head boundary. The figure also shows different values of penetration depths. The computational results of the peak values for SAR_{10g} and the corresponding numerical values of the penetration depth show the same effect of microwave frequency as presented by the contour distributions in fig. 6. It must be noted that the numerical value of the area under the line distribution of each frequency can be interpreted as proportional to the total energy absorption rate due to antenna microwave radiation propagating and penetrating within the solid angle subtended by the head boundary surface. The numerical value of the referred area can be calculated as the product of the average value of the line distribution and the value of the corresponding penetration length. Proceeding with the indicated numerical values of these quantities, one can obtain nearly equal products of about 400 W.mm/kg for all microwave frequencies. Keeping in mind that, the equal antenna microwave radiated power for all frequencies (1 W), this finding ensures the correctness of the solution for the microwave propagation and penetration.

In view of the 1-W antenna radiated power chosen for the present study as a worst condition, one must examine the safe situation associated with the antenna positioned in the voice calling position. This situation represents the use of the mobile phone at a specific frequency without any possible damaging effects on the human head. ICNIRP and IEEE standards specified the maximum allowable value of SAR_{10g} = 2 W/kg as a criterion for this safe situation. Comparing the peak values of SAR_{10g} indicated in fig. 8, the frequencies above 0.9 GHz exceed the safety limit of SAR_{10g} = 2 W/kg, and it is expected to cause physiological damage with long exposure time. To avoid such a condition, electromagnetic shielding can be used to keep SAR_{10g} below the safety limit [37].

Figure 9 shows nearly similar behavior of the peak temperature to those of the peak SAR_{10g} in fig. 8. However, there is significant difference regarding the value of the temperature-effective penetration depth at the end of which the temperature reaches the initial temperature of about 37.15 ℃. It is observed that all line distributions of the temperature show temperature-effective penetration depth with nearly equal value of 30 mm. This observation can be explained in view of the combined effect of the thermal energy generation rate due to microwave radiation and the thermophysical properties of the head tissues. Figure 10 shows the macroscale time variation of the temperature represented by the history of the instantaneous peak temperature rise within the total exposure time of 30 minutes. For all values of microwave frequencies of 0.9, 1.8 and 3 GHz, the temperature rapidly rises to nearly 63% of its final peak value in the first 6 minutes, while it slowly approaches this final value within the remaining 24 minutes of the total exposure time. This means that all the frequencies have the same time constant, which is the time needed for a response to reach 63.2% of its final value, of 6 minutes. This behavior of the peak temperature rise suggests that the reduction of the exposure time doesn't result in a significant favorable effect as that of the electromagnetic shielding.

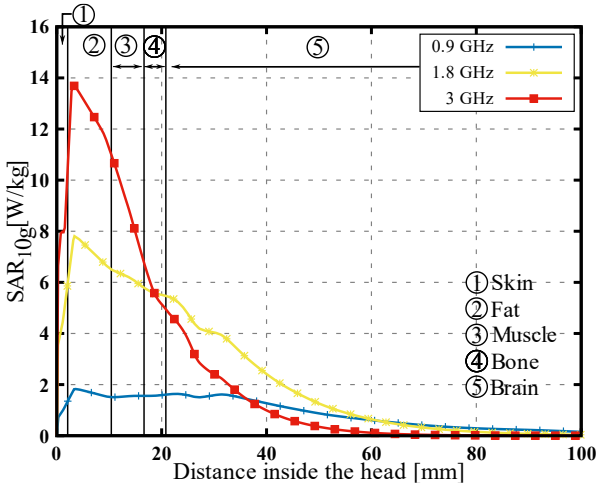

Fig. 8. Effect of microwave frequency on SAR_{10g} line distributions along a horizontal axis passing through the antenna center for the voice calling position.

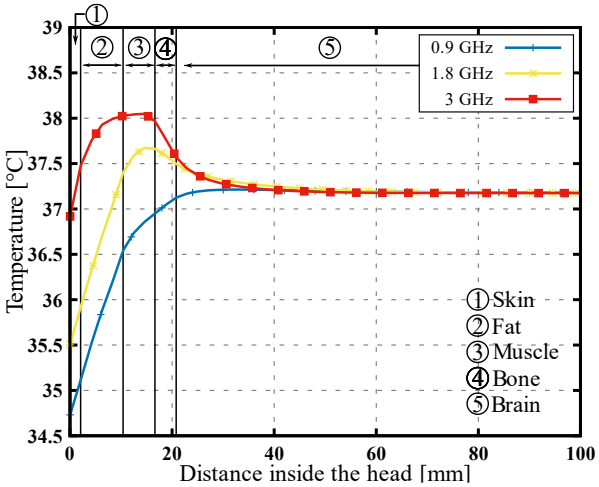

Fig. 9. Effect of microwave frequency on Temperature contour distributions along a horizontal axis for the video calling position at the end of 30-minute exposure time.

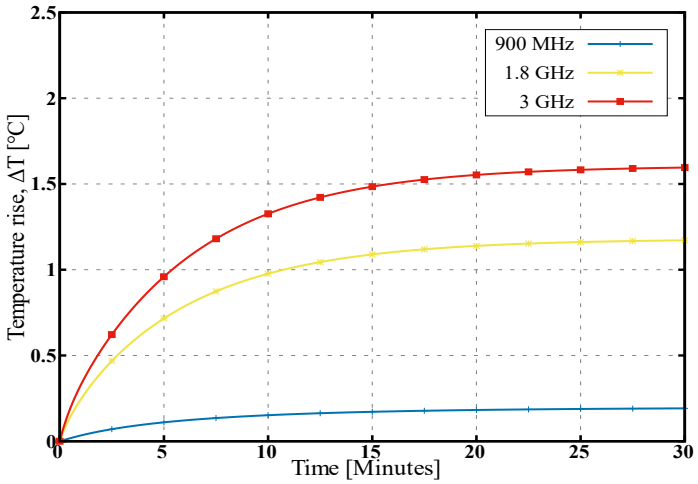

Fig. 10. Effect of microwave frequency on the time variation of the peak temperature rise in the voice calling position.

3.4 Bar Charts for The Status of Some Important Results

Figures 11 and 12 show the bar charts describing the status of the predictions for the peak values of SAR_{10g} and temperature rise. Figure 11 indicate that generally the microwave frequency increase has two counteracting effects on the peak SAR_{10g} values. The first effect is increasing the peak SAR_{10g} while the second effect is decreasing the associated penetration depth. Such counteracting effects possibly result in two different behaviors depending on the dielectric properties of the head model. The indicated value of the overall maximum SAR_{10g} (shown in blue) clearly shows a behavior of continuous increase up to a value of 14.9 W/kg as the frequency increases.

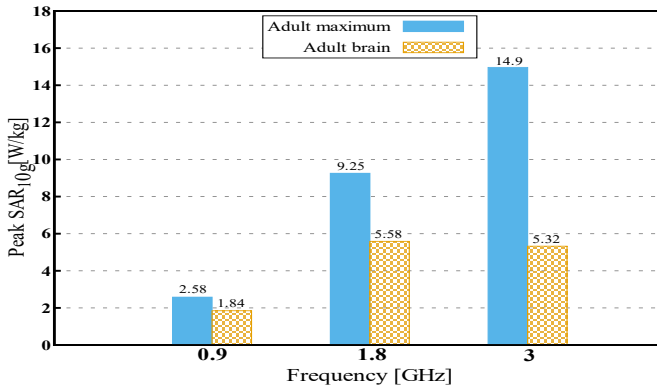

Fig. 11. Variation of peak SAR status with microwave frequency in the voice calling position.

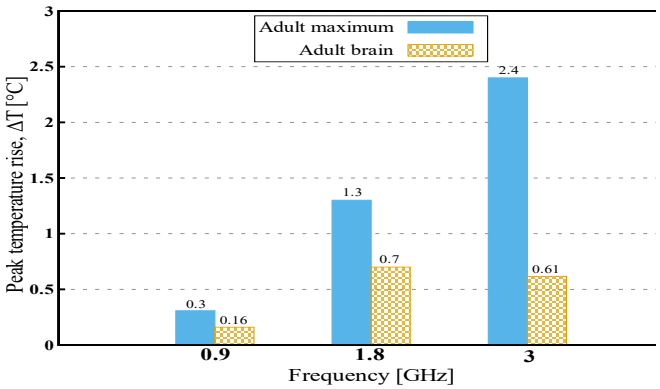

Fig. 12. Variation of the status for peak temperature rise with microwave frequency in the voice calling position.

On the other hand, the peak brain SAR_{10g} (shown in orange) are smaller compared to the overall peak value. it shows a behavior of an increase to a maximum of 5.58 W/kg at 1.8 GHz frequency. The indicated values of the peak temperature rise in fig. 12 show similar behaviors as those for the peak SAR_{10g} values. They are continuously increasing up to 2.4 ℃ for overall temperature rise. The temperature rises to a maximum of 0.7 ℃ inside the brain tissue.

4. Conclusion

In the present study, the effects of mobile phone radiation on human head model are studied. The influences of microwave frequency and mobile phone usage pattern (antenna-to-head position) are investigated. The human head details (structure and properties) were adopted according to the CST software package [35] and the standards of information technologies in society (IT'IS) [36]. The computational results of the mathematical model were obtained and presented to investigate important parameters such as SAR_{10g} and temperature rise. The results of a comparative study with other well-established solutions showed that a satisfactory verification with both correctness and calculations accuracy have been successfully achieved for the present numerical solution. The following important concluding remarks and findings were extracted based on the discussion of the investigated parameters:

- The numerical values of the SAR_{10g} and the corresponding temperatures with the antenna at the video calling position were found to be so small compared to the values at the voice calling position. The video calling position provided numerical SAR_{10g} values that are two orders of magnitude less than those of the voice calling position.
- The exposure to high frequency mobile phone radiation at 1 W antenna radiated power may result in peak SAR_{10g} value exceeding the international standard safety limit of 2 W/kg.
- Exposure to high frequency mobile phone radiation for about 6 minutes produces locally peak temperature rise values of 0.12 to 1 ℃ in the human head.

5. References

[1] ICNIRP. Guidelines for limiting exposure to electromagnetic fields (100 kHz to 300 GHz). Health Phys 118(00):000–000; 2020. Pre-print. https://doi.org/10.1097/HP.0000000000001210.

[2] IEEE Standard for Safety Levels with Respect to Human Exposure to Radio Frequency Electromagnetic Fields, 3 kHz to 300 GHz, *IEEE Std C95.1, 1999 Edition*, vol., no., pp.1-83, 16 April 1999, https://doi.org/10.1109/IEEESTD.1999.89423.

[3] A. C. Guyton, J. E. Hall, "Textbook of Medical Physiology," Philadelphia, PA, USA: Saunders, 2011.

[4] M. A. Stuchly, "Health effects of exposure to electromagnetic fields," IEEE Aerospace Applications Conference. Proceedings, 1995, pp. 351-368 vol.1, https://doi.org/10.1109/AERO.1995.468891.

[5] C. Chou, H. Bassen, J. Osepchuk, Q. Balzano, R. Petersen, M. Meltz, R. Cleveland, J. Lin, L. Heynick, "Radio frequency electromagnetic exposure: Tutorial review on experimental dosimetry," Bioelectromagnetics, (1996), 17: 195-208. https://doi.org/10.1002/(SICI)1521-186X(1996)17:3<195::AID-BEM5>3.0.CO;2-Z

[6] O. P. Gandhi, G. Lazzi, C. M. Furse, "Electromagnetic absorption in the human head and neck for mobile telephones at 835 and 1900 MHz," IEEE Transactions on Microwave Theory and Techniques, vol. 44, no. 10, pp. 1884-1897, Oct. 1996, https://doi.org/10.1109/22.539947.

[7] T. Ramachandran, M.R.I. Faruque, M.T. Islam, "Specific absorption rate reduction for sub-6 frequency range using polarization dependent metamaterial with high effective medium ratio," Sci Rep 12, 1803 (2022). https://doi.org/10.1038/s41598-022-05851-2

[8] H. Ben Hamadi, S. Ghnimi, L. Latrach, P. Benech, A. Gharsallah, "New Design of Multi-Band PIFA Antenna with Reduced SAR for Mobile and Wireless Applications," Wireless Pers Commun 115, 1211–1226 (2020). https://doi.org/10.1007/s11277-020-07619-1

[9] A. Hadjem, E. Conil, A. Gati, M. Man-Faï Wong, J. Wiart, "Analysis of Power Absorbed by Children's Head as a Result of New Usages of Mobile Phone," IEEE Transactions on Electromagnetic Compatibility, vol. 52, no. 4, pp. 812-819, Nov. 2010, https://doi.org/10.1109/TEMC.2010.2052810.

[10] MI. Hossain, MR. Faruque, MT. Islam, "Analysis on the effect of the distances and inclination angles between human head and mobile phone on SAR," Prog. Biophys Mol Biol. Nov 2015 ;119(2):103-10. https://doi.org/10.1016/j.pbiomolbio.2015.03.008.

[11] M. Martínez-Búrdalo, A. Martín, M. Anguiano, R. Villar, "Comparison of FDTD-calculated specific absorption rate in adults and children when using a mobile phone at 900 and 1800 MHz," Phys Med Biol. Jan 2004 21;49(2):345-54. https://doi.org/10.1088/0031-9155/49/2/011.

[12] J. Wang, O. Fujiwara, "Comparison and evaluation of electromagnetic absorption characteristics in realistic human head models of adult and children for 900-MHz mobile telephones," IEEE Transactions on Microwave Theory and Techniques, vol. 51, no. 3, pp. 966-971, March 2003, https://doi.org/10.1109/TMTT.2003.808681.

[13] AA. de Salles, G. Bulla, CE. Rodriguez, "Electromagnetic absorption in the head of adults and children due to mobile phone operation close to the head," Electromagn Biol Med. 2006;25(4):349-60. https://doi.org/10.1080/15368370601054894.

[14] J. Keshvari, S. Lang, "Comparison of radio frequency energy absorption in ear and eye region of children and adults at 900, 1800 and 2450 MHz," Phys Med Biol. Sep 2005 21;50(18):4355-69. https://doi.org/10.1088/0031-9155/50/18/008.

[15] T. Wessapan, P. Rattanadecho, "Numerical Analysis of Specific Absorption Rate and Heat Transfer in Human Head Subjected to Mobile Phone Radiation: Effects of User Age and Radiated Power," ASME. *J. Heat Transfer*. December 2012; 134(12): 121101. https://doi.org/10.1115/1.4006595

[16] A. Hirata, Y. Diao, T. Onishi, K. Sasaki, S. Ahn, D. Colombi, V. D. Santis, I. Laakso, L. Giaccone, W. Joseph, E. A. Rashed, W. Kainz, J. Chen "Assessment of Human Exposure to Electromagnetic Fields: Review and Future Directions," IEEE Transactions on Electromagnetic Compatibility, vol. 63, no. 5, pp. 1619-1630, Oct. 2021, https://doi.org/10.1109/TEMC.2021.3109249

[17] F. Kaburcuk, A. Z. Elsherbeni, "Temperature Rise and SAR Distribution at Wide Range of Frequencies in a Human Head due to an Antenna Radiation," ACES Journal, vol. 33, no. 04, pp. 367–372, Jul. 2021

[18] M. Cavagnaro and J. C. Lin, "Importance of Exposure Duration and Metrics on Correlation Between RF Energy Absorption and Temperature Increase in a Human Model," IEEE Transactions on Biomedical Engineering, vol. 66, no. 8, pp. 2253-2258, Aug. 2019, https://doi.org/10.1109/TBME.2018.2886475

[19] S. Iman Zonoori, S. Vahab Al-Din Makki, A. Torabi, "A Comparative study of the distance effects of human head from mobile phone radiation," International Journal of Microwave and Optical Technology, vol. 10, no. 1, January 2015

[20] T. Wessapan, P. Rattanadecho, "Specific absorption rate and temperature increase in the human eye due to electromagnetic fields exposure at different frequencies," International Journal of Heat and Mass Transfer, Volume 64, 2013, Pages 426-435, ISSN 0017-9310, https://doi.org/10.1016/j.ijheatmasstransfer.2013.04.060.

[21] H. H. Zhang, Z. C. Lin, W. E. I. Sha, W. W. Choi, K. W. Tam, D. G. Donoro, G. Shi, "Electromagnetic-Thermal Analysis of Human Head Exposed to Cell Phones With the Consideration of Radiative Cooling," IEEE Antennas and Wireless Propagation Letters, vol. 17, no. 9, pp. 1584-1587, Sept. 2018, https://doi.org/10.1109/LAWP.2018.2856365.

[22] P. Bernardi, M. Cavagnaro, S. Pisa, E. Piuzzi, "Specific absorption rate and temperature increases in the head of a cellular-phone user, IEEE Transactions on Microwave Theory and Techniques," vol. 48, no. 7, pp. 1118-1126, July 2000, https://doi.org/10.1109/22.848494.

[23] A. Siriwitpreecha, P. Rattanadecho, T. Wessapan, "The influence of wave propagation mode on specific absorption rate and heat transfer in human body exposed to electromagnetic wave," International Journal of Heat and Mass Transfer, 65, (2013), 423–434. https://doi.org/10.1016/j.ijheatmasstransfer.2013.06.015

[24] B. Rajagopal, L. Rajasekaran, "SAR assessment on three layered spherical human head model irradiated by mobile phone antenna," Hum. Cent. Comput. Inf. Sci. 4, 10 (2014). https://doi.org/10.1186/s13673-014-0010-1

[25] D. Bhargava, N. Leeprechanon, P. Rattanadecho, T. Wessapan, "Specific absorption rate and temperature elevation in the human head due to overexposure to mobile phone radiation with different usage patterns," International Journal of Heat and Mass Transfer, 130, (2019), 1178–1188. https://doi.org/10.1016/j.ijheatmasstransfer.2018.11.031

[26] Stanković, V., Jovanović, D., Krstić, D., Marković, V., & Cvetković, N. (2017). "Temperature distribution and Specific Absorption Rate inside a child's head," International Journal of Heat and Mass Transfer, 104, 559– 565. https://doi.org/10.1016/j.ijheatmasstransfer.2016.08.094

[27] T. Wessapan, P. Rattanadecho, "Temperature induced in human organs due to near-field and far-field electromagnetic exposure effects," International Journal of Heat and Mass Transfer, 119, 65–76. (2018) https://doi.org/10.1016/j.ijheatmasstransfer.2017.11.088

[28] R. Seetharaman, M. Tharun, S. Gayathri, S.S.Sreeja Mole, K. Anandan, "Analysis of specific absorption rate and heat transfer in human head due to mobile phones," Materials Today: Proceedings, Volume 51, Part 8, 2022, https://doi.org/10.1016/j.matpr.2021.11.582

[29] Z.M. Lwin, M. Yokota, "Numerical analysis of SAR and temperature distribution in two dimensional human head model based on FDTD parameters and the polarization of electromagnetic wave," AEU - International Journal of Electronics and Communications, Volume 104, 2019, https://doi.org/10.1016/j.aeue.2019.03.010

[30] J. C. Maxwell, "A Dynamical Theory of the Electromagnetic Field," in W. D. Niven (ed.), The Scientific Papers of James Clerk Maxwell, vol. 1, Cambridge University Press, London, 1890.

[31] M. Born, E. Wolf, "Principles of Optics: Electromagnetic Theory of Propagation Interference and Diffraction of Light," 6th edition, Butterworth-Heinemann; (December 1980)

[32] M. Clemens, T. Weiland, "Discrete Electromagnetism with the Finite Integration Technique," Progress In Electromagnetics Research, Vol. 32, 65-87, 2001. https://doi.org/10.2528/PIER00080103

[33] HH. Pennes, "Analysis of tissue and arterial blood temperatures in the resting human forearm," 1948. J Appl Physiol (1985). 1998 Jul;85(1):5-34. https://doi.org/10.1152/jappl.1998.85.1.5.

[34] D. Fiala, KJ. Lomas, M. Stohrer, "A computer model of human thermoregulation for a wide range of environmental conditions: the passive system," J Appl Physiol (1985). 1999 Nov;87(5):1957-72. https://doi.org/10.1152/jappl.1999.87.5.1957.

[35] "CST Studio Suite®" 2020, https://www.3ds.com/products-services/simulia/products/cst-studio-suite/

[36] PA. Hasgall, F. Di Gennaro, C. Baumgartner, E. Neufeld, B. Lloyd, MC. Gosselin, D. Payne, A. Klingenböck, N. Kuster, "IT'IS Database for thermal and electromagnetic parameters of biological tissues," Version 4.0, May 2018, https://doi.org/10.13099/VIP21000-04-0. itis.swiss/database

[37] S. Nishizaw, O. Hashimoto, "Effectiveness analysis of lossy dielectric shields for a three-layered human model," IEEE Transactions on Microwave Theory and Techniques, 47(3), (1999), 277–283. https://doi.org/10.1109/22.750223

[38] J. R. Howell, R. Siegel, M. P. Mengüc, "Thermal Radiation Heat Transfer," 5th Edition, CRC Press, (2010)

نمذجة حسابية واقعية للتأثيرات البايولوجية الحرارية داخل رأس الانسان المعرض لإشعاع الهاتف المحمول

الملخص بالعربى

في الآونة الأخيرة أدى تطور الهواتف الذكية مع ظهور أجيال جديدة من شبكات الهاتف المحمول إلى انتشار مخاوف كثيرة بين المستخدمين من تأثير التعرض المستمر لإشعاع هذه الهواتف على أعضاء الانسان الحساسة. تقوم الدراسة الحالية بفحص توزيع كلًا من معدل الامتصاص النوعي ودرجة الحرارة داخل نموذج فيزيائي تشريحي دقيق لرأس الانسان المعرض لإشعاع الهاتف المحمول. يتم حل المعادلات الحاكمة عدديًا لفحص أثر حالات مختلفة على هذه التوزيعات. من هذه الحالات تردد إشعاع الهاتف المحمول وهي ٠,٩ و١,٨ و٣ جيجاهرتز بالاضافة إلى حالتي الاتصال الصوتي والمرئي لكشف أثر موقع الهاتف بالنسبة لرأس الانسان. كما تضمنت الدراسة توثيق صحة ودقة الحل العددي من خلال المقارنة مع حلول مرجعية منشورة. وأظهرت النتائج أن القيم القصوى لمعدل الامتصاص النوعي وارتفاع درجة الحرارة كانت في حالة الاتصال الصوتي عند تردد ٣ جيجاهرتز بقيم مقدارها ١٤,٩ وات/كيلوجرام و ١,٦ درجة سيليزية على التوالي. أوضحت النتائج – أيضًا – أن قيم كلًا من معدل الامتصاص النوعي ودرجة الحرارة المتعلقة بحالة الاتصال المرئي صغيرة جدًا ويمكن تجاهلها. كما بينت النتائج أن درجة الحرارة تتجاوز ٦٣٪ من قيمتها النهائية في خلال ٦ دقائق لكل الترددات المختلفة لإشعاع الهاتف المحمول.

الكلمات الرئيسية

إشعاع كهرومغناطيسي، إنتقال حرارة، توزيع درجة الحرارة، رأس الانسان، هاتف محمول